Proton-coupled electron transfer of macrocyclic ring hydrogenation: The chlorinphlorin

Rui Sun, Mengran Liu, Shao-Liang Zheng, Dilek K Dogutan, Cyrille Costentin, Daniel G Nocera

▶ **To cite this version:**

Rui Sun, Mengran Liu, Shao-Liang Zheng, Dilek K Dogutan, Cyrille Costentin, et al.. Proton-coupled electron transfer of macrocyclic ring hydrogenation: The chlorinphlorin. Proceedings of the National Academy of Sciences of the United States of America, 2022, 119 (20), pp.e2122063119. 10.1073/pnas.2122063119 . hal-04689526

HAL Id: hal-04689526
https://hal.science/hal-04689526v1

Submitted on 5 Sep 2024

HAL is a multi-disciplinary open access archive for the deposit and dissemination of scientific research documents, whether they are published or not. The documents may come from teaching and research institutions in France or abroad, or from public or private research centers.

L'archive ouverte pluridisciplinaire **HAL**, est destinée au dépôt et à la diffusion de documents scientifiques de niveau recherche, publiés ou non, émanant des établissements d'enseignement et de recherche français ou étrangers, des laboratoires publics ou privés.

Distributed under a Creative Commons Attribution 4.0 International License

PNAS RESEARCH ARTICLE | CHEMISTRY

Proton-coupled electron transfer of macrocyclic ring hydrogenation: The chlorinphlorin

Rui Sun[a,1], Mengran Liu[a,1], Shao-Liang Zheng[a], Dilek K. Dogutan[a,2], Cyrille Costentin[b,c,2], and Daniel G. Nocera[a,2]

Contributed by Daniel G. Nocera; received December 6, 2021; accepted March 7, 2022; reviewed by Jillian Dempsey and Jenny Yang

Redox noninnocence of pyrrole macrocycles allows for their hydrogenation by proton-coupled electron transfer (PCET). The initial reduction of porphyrins by PCET occurs at a bridging methine carbon, yielding a phlorin. In macrocyclic cores that are reduced beyond porphyrins, the phlorin is unusual. The chlorinphlorin is an especially rare compound, and consequently, its formation and chemistry have eluded characterization. We now report the chemical preparation of a chlorinphlorin, including its X-ray crystal structure, which is distinguished by a tetrahedral geometry about the methine carbon of the macrocycle, resulting in the formal reduction of an olefin bond. We establish that the reductive electrochemistry of a series of hangman chlorins furnishes the chlorinphlorin by electrochemical hydrogenation according to a PCET mechanism. The rate constant for proton transfer from the pendant acid in the secondary coordination sphere to the chlorin anion radical is 10^3 s^{-1}. This initial proton transfer forms the N–H bond of the chlorinphlorin; upon a second reduction, the C–H bond at the tetrahedral methine bridge is formed. In the presence of exogenous acid, the hangman group prepositions the acid to trigger a concerted PCET reaction, thereby bypassing the chlorin anion radical intermediate. When the chlorin macrocycle is metalated, the formation of the initial N–H bond is prevented, and the hydrogenation of the chlorin macrocycle by PCET leads to the isobacteriochlorin.

chlorin | PCET | hydrogenation | porphyrin | chlorinphlorin

Significance

The chemical reduction of unsaturated bonds occurs by hydrogenation with H_2 as the reductant. Conversely, in biology, the unavailability of H_2 engenders the typical reduction of unsaturated bonds with electrons and protons from different cofactors, requiring olefin hydrogenation to occur by proton-coupled electron transfer (PCET). Moreover, the redox noninnocence of tetrapyrrole macrocycles furnishes unusual PCET intermediates, including the phlorin, which is an intermediate in tetrapyrrole ring reductions. Whereas the phlorin of a porphyrin is well established, the phlorin of a chlorin is enigmatic. By controlling the PCET reactivity of a chlorin, including the use of a hangman functionality to manage the proton transfer, the formation of a chlorinphlorin by PCET is realized, and the mechanism for its formation is defined.

Hydrogenation of unsaturated compounds is a common transformation in chemistry and biology, but the reaction typically occurs by different mechanisms. Whereas chemical hydrogenation usually relies on H_2 as the reductant, nature uses enzymes to form saturated bonds with electrons provided from a redox cofactor and protons from prepositioned donors. For instance, in anoxygenic photosynthetic bacteria, biohydrogenation of chlorophyll to bacteriochlorophyll is performed by a chlorophyllide oxidoreductase, with two electrons provided by a reduced ferredoxin and two protons provided by peptidyl residues proximate to the active site (1). Similarly, hydrogenation by the dark-operative protochlorophyllide oxidoreductase, which reduces protochlorophyllide (a heme derivative) to form a direct precursor of chlorophyll *a* in a light-independent route, is accomplished with electrons from an Fe_4S_4 cluster coupled to proton transfers from intramolecular propionic acid and a nearby aspartate (2).

The chemical reduction of unsaturated olefin bonds by proton-coupled electron transfer (PCET) occurs at high potential and is a kinetically cumbersome transformation (3) that is avoided when H_2 is the reductant. However, in biological reductions, the different sources of the electron and proton impose that the hydrogenation of the olefin bond occurs by PCET. Multisite PCET hydrogenations of the unsaturated bonds of biological macrocycles can give rise to unusual macrocyclic cores that are not accessible by direct reduction. Such PCET reactivity is generally derived from redox noninnocence of ligands (4). Hydrogenation of an olefin moiety involving the methine carbon in a porphyrin ring gives rise to phlorins, which are an initial intermediate in the formation of chlorins (hydrogenation of one C_β–C_β bond) (Fig. 1) and are also found as intermediates in porphyrin catalysis of the hydrogen evolution reaction (5, 6). In macrocyclic cores that are reduced beyond porphyrins, the phlorin is more enigmatic. Whereas the methine positions next to the pyrroline ring of a chlorin have higher electron density and thus, are susceptible to electrophilic attack, the chlorinphlorin has nevertheless been elusive (Fig. 1). The only reports of chlorinphlorin describe its generation from electrochemical (7, 8) or photochemical (9, 10) reduction of chlorophyll-related parent molecules. The oddity of chlorinphlorin (11) has resulted in its inadequate characterization, which has been restricted to a single broad absorption trace (11) and ^{1}H NMR spectra (7, 9). In addition to the fundamental interest in the formation of a chlorinphlorin from PCET reduction of the chlorin macrocycle, the hydrogenation of the chlorin ring is intriguing because the chemistry of reduced

Author contributions: D.K.D., C.C., and D.G.N. designed research; R.S. and M.L. performed research; R.S., M.L., S.-L.Z., and C.C. contributed new reagents/analytic tools; R.S., S.-L.Z., D.K.D., C.C., and D.G.N. analyzed data; and R.S., D.K.D., C.C., and D.G.N. wrote the paper.

Reviewers: J.D., The University of North Carolina at Chapel Hill; and J.Y., University of California, Irvine.

The authors declare no competing interest.

Copyright © 2022 the Author(s). Published by PNAS. This article is distributed under Creative Commons Attribution-NonCommercial-NoDerivatives License 4.0 (CC BY-NC-ND).

[1]R.S. and M.L. contributed equally to this work.

[2]To whom correspondence may be addressed. Email: dkiper@fas.harvard.edu, cyrille.costentin@univ-grenoble-alpes.fr, or dnocera@fas.harvard.edu.

This article contains supporting information online at http://www.pnas.org/lookup/suppl/doi:10.1073/pnas.2122063119/-/DCSupplemental.

Published May 9, 2022.

Downloaded from https://www.pnas.org by Univ Joseph Fourier/INPG on September 5, 2024 from IP address 152.77.14.50.

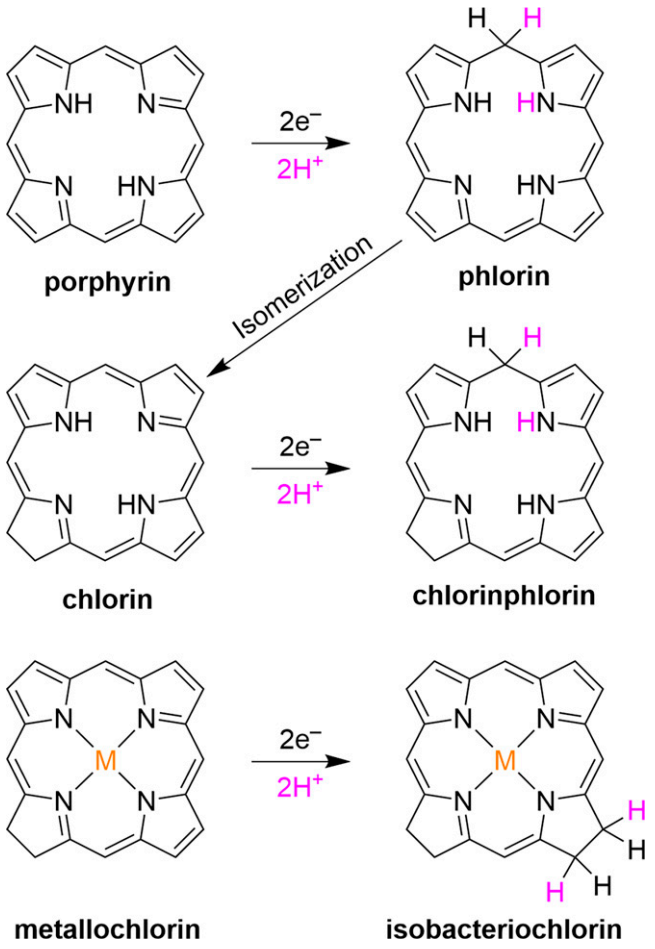

Fig. 1. Reduction of tetrapyrrole macrocyclic rings to produce phlorin, chlorinphlorin, and isobacteriochlorin.

chlorins is the keystone to the biosynthesis of bacteriochlorophylls (12, 13). Accordingly, an understanding of the multisite PCET hydrogenation of chlorin to chlorinphlorin is valuable and more generally, provides insight into the reduction of unsaturated carbon–carbon bonds by PCET in biology.

Hangman macrocyclic platforms offer the opportunity to examine hydrogenation by multisite PCET with structural and mechanistic precision. Such reactivity is conveniently probed with electrochemistry, which has been shown to be a useful technique for the investigation of PCET mechanisms (14) and indeed, has been employed to study the reduction of aromatic hydrocarbons in the presence of proton donors, which has been shown to occur stepwise (15). In contrast, concerted proton–electron transfer (CPET) has been shown to be a viable pathway for polar bonds where prepositioning of the reactants through hydrogen bonding is a prerequisite for CPET to occur (16). Accordingly, the hangman architecture of chlorin provides a path to macrocyclic hydrogenation by CPET as proton donors may be positioned within the hangman cleft of the chlorin macrocycle for the study of its electrochemical hydrogenation.

Here, we investigate the electrochemical reduction of the hangman chlorins shown in Fig. 2. In addition to the two hangman chlorin isomers with a xanthene backbone and a

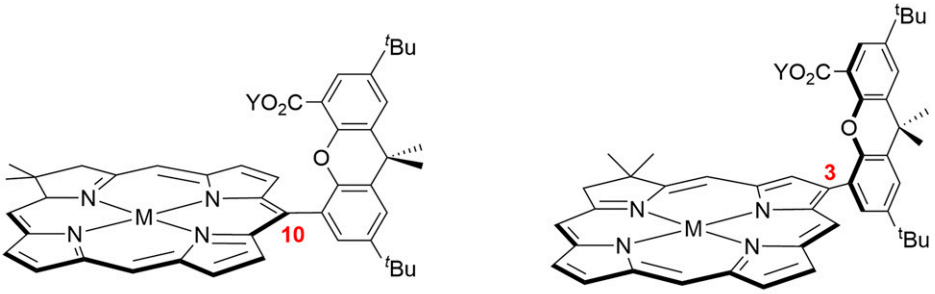

H_2CX^{10}-H (M = H, H; Y = H)
$ZnCX^{10}$-H (M = Zn; Y = H)
H_2CX^{10}-Me (M = H, H; Y = CH_3)
$ZnCX^{10}$-Me (M = Zn; Y = CH_3)

H_2CX^{3}-H (M = H, H; Y = H)
$ZnCX^{3}$-H (M = Zn; Y = H)
H_2CX^{3}-Me (M = H, H; Y = CH_3)
$ZnCX^{3}$-Me (M = Zn; Y = CH_3)

Fig. 2. Hangman chlorins with pendant acid and ester groups.

Downloaded from https://www.pnas.org by Univ Joseph Fourier/INPG on September 5, 2024 from IP address 152.77.14.50.

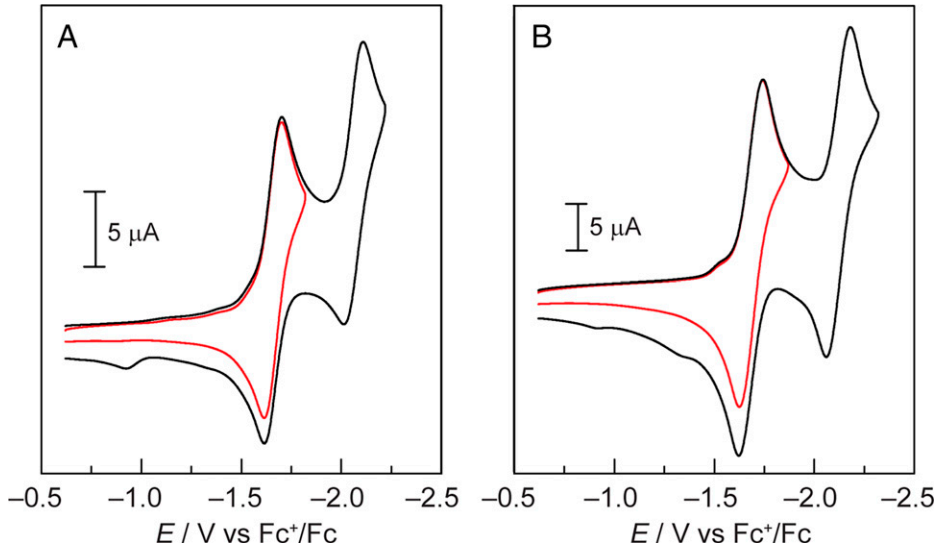

Fig. 3. CVs of (*A*) **H_2CX^3-Me** (1 mM) and (*B*) **H_2CX^{10}-Me** (1.55 mM) measured in anhydrous acetonitrile with *n*-Bu_4NPF_6 as the supporting electrolyte (0.1 M) using a 3-mm glassy carbon working electrode. v = 0.1 V/s.

pendant carboxylic acid at either the 3 or the 10 position, the hangman compounds with the corresponding pendant esters have been prepared in order to elucidate the role of hydrogen bonding in promoting electrochemical reduction of the chlorin. Quantitative analysis of the cyclic voltammograms (CVs) along with spectroelectrochemical data allows us to propose mechanisms and evaluate rate constants. We show that there is a "synergetic" effect between exogenous benzoic acid and the pendant carboxylic group, thereby making the PCET reduction easier than the reduction of the corresponding chlorins containing ester pendant groups and opening a route for a CPET pathway to form the N–H bond (and subsequently, the C–H bond of the chlorinphlorin). This CPET pathway is circumvented when a nonelectroactive cation, Zn^{2+}, is introduced into the chlorin cavity, which blocks N–H bond formation and in doing so, redirects the hydrogenation of the chlorin to furnish isobacteriochlorin (Fig. 1).

Results and Discussion

The hangman chlorins shown in Fig. 2 feature a *gem*-dimethyl group at the 18 position to lock the structure of the macrocycle and increase its stability toward oxidation. The compounds functionalized at the 10 position shown in Fig. 2 were prepared by the previously described preinstallation approach where the xanthene backbone is incorporated at the *meso* position of the bispyrrole prior to the condensation reaction to form the chlorin macrocycle (17). Those functionalized at the 3 position were prepared by the postinstallation approach, where a Pd-mediated Suzuki–Miyaura cross-coupling was used to install the xanthene backbone after macrocycle formation. The characterization of the compounds in Fig. 2 was in accordance with the published data (17).

Chlorin Reduction in the Absence of Exogenous Acid. The methyl hangman substitution (Y = CH_3) allows the redox chemistry of the hangman chlorin to be determined in the absence of PCET. CVs of chlorins **H_2CX^3-Me** and **H_2CX^{10}-Me** are shown in Fig. 3. Consistent with tetraphenylchlorin (18), the hangman compounds exhibit two reversible waves corresponding to the formation of the mono- and direduced forms of the chlorins, characterized by the standard potentials E_1^0 and E_2^0 given in Table 1. Similar CVs are obtained with **$ZnCX^3$-Me** and **$ZnCX^{10}$-Me** (*SI Appendix*, Fig. S7), although the standard potentials are cathodically shifted by 200 mV for E_1^0 and 100 mV for E_2^0 (Table 1). Indeed, thin-layer spectroelectrochemistry of **$ZnCX^3$-Me** (*SI Appendix*, Fig. S1*A*) and **$ZnCX^{10}$-Me** (*SI Appendix*, Fig. S1*B*) at a potential of –2.00 V vs. Fc^+/Fc (ferrocene) leads to the formation of the one-electron reduced species, **$Chl^{\bullet-}$** (18); the same **$Chl^{\bullet-}$** spectrum is observed for **H_2CX^3-Me** (*SI Appendix*, Fig. S1*C*) and **H_2CX^{10}-Me** (*SI Appendix*, Fig. S1*D*) in the absence of benzoic acid.

The hangman chlorins **H_2CX^3-H** and **H_2CX^{10}-H** exhibit more complicated CVs (Fig. 4) due to the pendant acid functionality. The CVs are consistent with the ECE (E, electron transfer step; C, chemical step) mechanism shown in Scheme 1. Within this framework, the first cathodic wave involves electron transfer (characterized by a standard potential E_3^0) to furnish the chlorin anion radical followed by an intramolecular irreversible proton transfer (characterized by a first-order rate constant k_{PT}). This subsequent radical is reversibly reduced at a more negative potential (E_4^0).

The E_3^0 and E_1^0 values for the Y = H and Me chlorins are assumed to be similar as the pendant proton should have little effect on the porphyrin frontier orbitals and thus, on the potential of the first cathodic process to produce the radical anion (Table 1). However, this is not the case for the second electron

Table 1. Standard potentials (V vs. Fc^+/Fc) and intramolecular proton transfer rate constants ($seconds^{-1}$)

	H_2CX^{10}-Y	$ZnCX^{10}$-Y	H_2CX^3-Y	$ZnCX^3$-Y
Y = Me				
E_1^0	−1.68	−1.88	−1.65	−1.86
E_2^0	−2.12	−2.22	−2.05	−2.16
Y = H				
E_3^0	−1.68	−1.88	−1.65	−1.86
E_4^0	−1.74	−2.01	−1.74	−1.93
k_{PT}	10^3	2×10^2	10^3	50

Downloaded from https://www.pnas.org by Univ Joseph Fourier/INPG on September 5, 2024 from IP address 152.77.14.50.

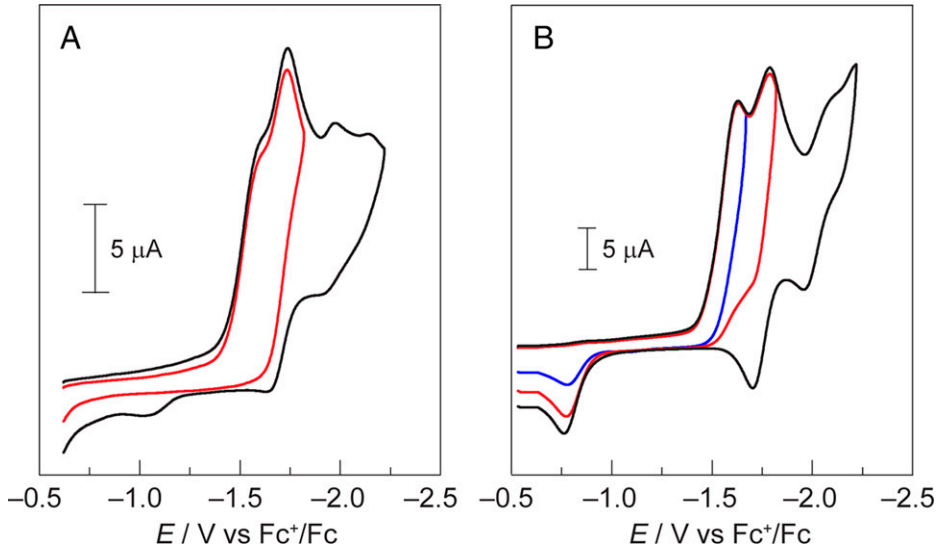

Fig. 4. CVs of (*A*) **H_2CX^3-H** (1 mM) and (*B*) **H_2CX^{10}-H** (2 mM) measured in anhydrous acetonitrile with *n*-Bu_4NPF_6 as the supporting electrolyte (0.1 M) using a 3-mm glassy carbon working electrode. v = 0.1 V/s.

reduction. E_4^0 is more positive than E_2^0 (200 to 300 mV) (Table 1) and only 80 to 90 mV more negative of E_1^0 due to proton transfer from the hangman group, which neutralizes the charge on the chlorin ring. However, in contrast to the classical ECE disproportionation mechanism (19) (where the C step is a bimolecular protonation, an addition of an electrophile to the anion radical, or bond cleavage in the anion radical), the second electron transfer occurs at more negative potential of the first arising from the residual negative charge on the hangman carboxylate. Consequently, the disproportionation reaction (i.e., a bimolecular reaction between the two anion radicals involved in the proton transfer step) is thermodynamically unfavorable, in contrast to the classical mechanism for electrochemical hydrogenation of aromatic hydrocarbons in the presence of an external proton source (20). The intramolecular proton transfer rate constant k_{PT} is obtained from the first irreversible peak potential according to

$$E_p = E_3^0 - 0.78\frac{RT}{F} + \frac{RT}{2F}\ln\left(\frac{RT}{Fv}k_{PT}\right), \qquad [1]$$

where proton transfer is assumed to be fast and irreversible, thus corresponding to "pure kinetic" conditions where the initial one-electron reduced **$Chl^{\bullet-}$** does not accumulate because it is at steady state in a very thin diffusion–reaction layer due to mutual compensation between its diffusion from the electrode surface where it is produced and its rapid intramolecular protonation (19). The obtained rate constants (Table 1) are indeed consistent with a large kinetic parameter $\lambda = \frac{RT}{Fv}k_{PT} \gg 1$, which is a measure of the competition between the intramolecular protonation and the timescale of the CV, thereby validating this assumption. Qualitatively similar behaviors were observed with **$ZnCX^{10}$-H** and **$ZnCX^3$-H**, but the internal proton transfers are slower (Table 1).

As shown in Fig. 4, the CVs of the hangman free base compounds exhibit an additional cathodic feature. A reversible wave is observed at a more negative potential of the second electron reduction (e.g., –1.98 and –2.03 V vs. Fc^+/Fc for **H_2CX^3-H** and **H_2CX^{10}-H**, respectively) that is ascribed to further reduction of the chlorin macrocycle (E_5^0 in Scheme 1). **H_2CX^{10}-H** also exhibits an anodic irreversible wave at –0.75 V vs. Fc^+/Fc. As demonstrated by a CV where the potential is reversed just negative of the first wave (blue trace in Fig. 4*B*), this anodic wave corresponds to the oxidation of a species formed at the level of the first wave. We suspect that the radical formed upon the initial reduction and subsequent intramolecular PCET is partially protonated at the carboxylate (either from trace acid or from another molecule of substrate). The resulting neutral radical is then immediately reduced (ECE process), leading to a more stabilized anion whose reoxidation is then observed at ~ –0.75 V vs. Fc^+/Fc for **H_2CX^{10}-H**. This second reduction is in competition with a fast chemical step, as attested by the irreversibility of the reoxidation wave (*SI Appendix*, Fig. S2).

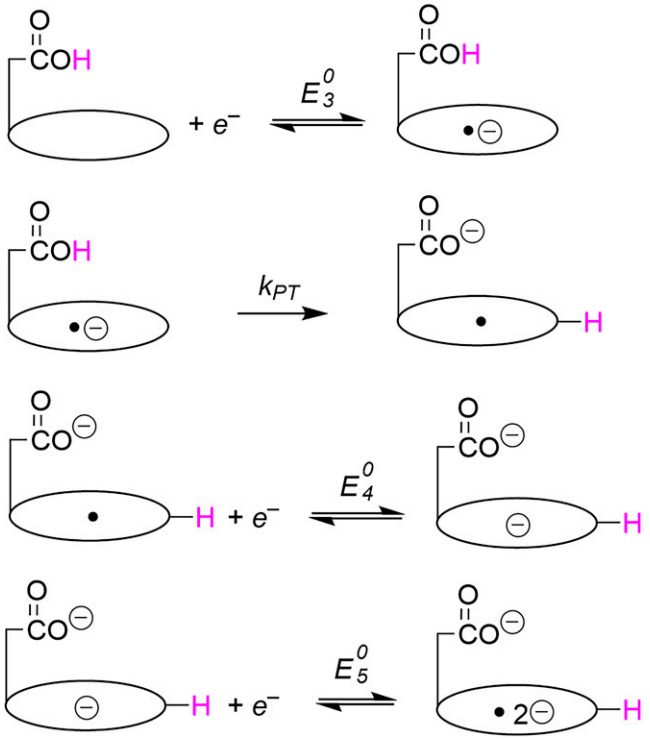

Scheme 1. Overall mechanism for hangman acid–functionalized chlorin reduction.

Chlorin Reduction in the Presence of Exogenous Acid. To investigate the mechanism of electrochemical hydrogenation of

Downloaded from https://www.pnas.org by Univ Joseph Fourier/INPG on September 5, 2024 from IP address 152.77.14.50.

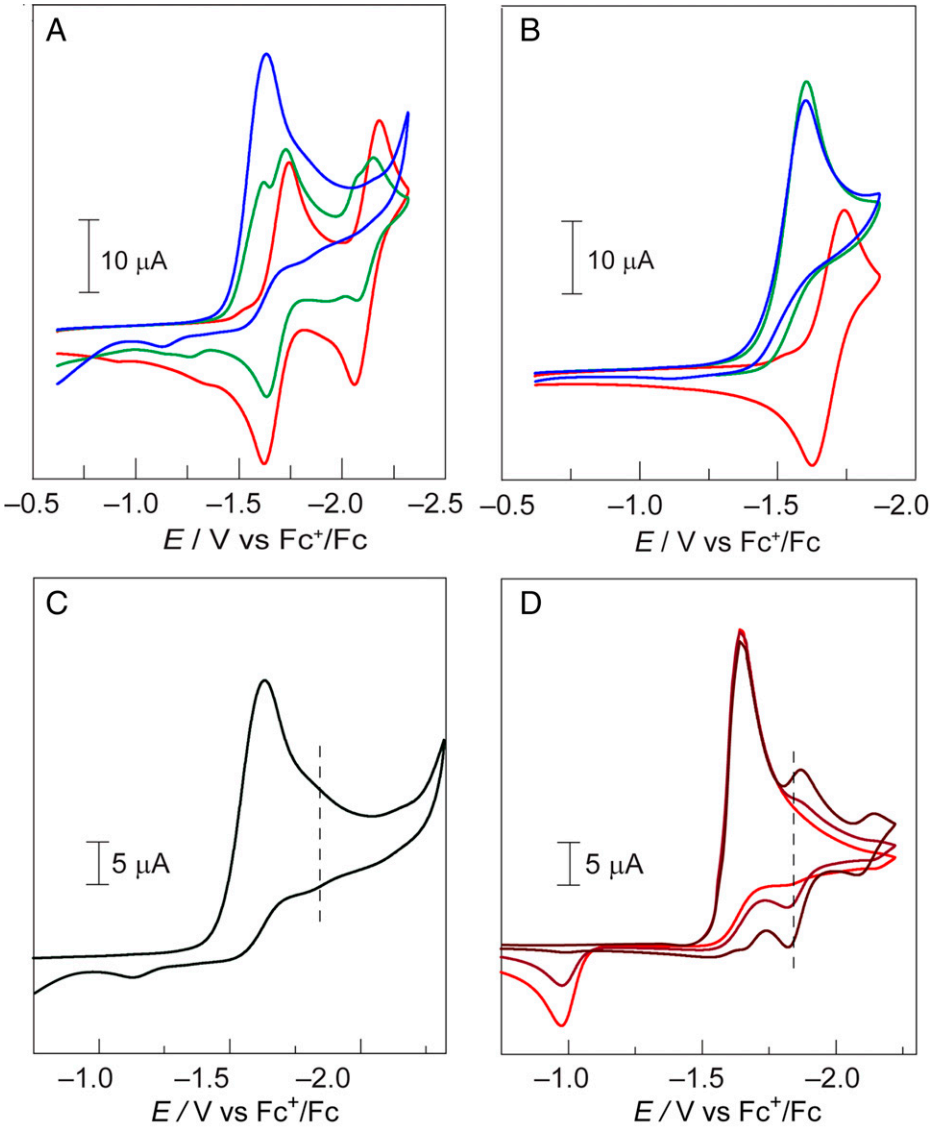

Fig. 5. CVs of $\mathbf{H_2CX^{10}}$**-Me** (1.6 mM) in the presence of benzoic acid at concentrations of (*A*) 0 mM (red), 0.5 mM (green), and 2 mM (blue) and for (*B*) 0 mM (red), 5 mM (green), and 20 mM (blue). (*C*) CV of $\mathbf{H_2CX^{10}}$**-Me** (1.6 mM) in the presence of 2 mM benzoic acid. (*D*) Simulated CVs of $\mathbf{H_2CX^{10}}$**-Me** (1.6 mM) in the presence of 2 mM benzoic acid with k_{H2} = 10 M^{-1} s^{-1} (red), 100 M^{-1} s^{-1} (burgundy), and 1,000 M^{-1} s^{-1} (brick red). The dotted vertical lines indicate the location of the **Chl(H_2)** reduction wave. The simulation reproduces experimental CV for k_{H2} = 10 M^{-1} s^{-1}. All CVs were taken in anhydrous acetonitrile with *n*-Bu_4NPF_6 as the supporting electrolyte (0.1 M) using a 3-mm glassy carbon working electrode. v = 0.1 V/s.

chlorins containing a pendant methyl ester group, CVs of $\mathbf{H_2CX^3}$**-Me** and $\mathbf{H_2CX^{10}}$**-Me** were recorded with increasing amounts of benzoic acid (pK_a = 20 in acetonitrile) (21). As shown in Fig. 5, the presence of a weak acid significantly perturbs the CVs. At low acid concentrations (Fig. 5*A* and *SI Appendix*, Fig. S3*B* for $\mathbf{H_2CX^{10}}$**-Me**), the second reversible wave decreases simultaneously with the increase of the first wave, and a small quasireversible wave appears at an intermediate potential (~ −1.85 V vs. Fc^+/Fc) (dotted line in Fig. 5*C*). As the acid concentration is increased (Fig. 5*B* and *SI Appendix*, Fig. S3*D* for $\mathbf{H_2CX^{10}}$**-Me**), the first wave slightly shifts anodically by roughly $\partial E_p/\partial \log[AH] \sim 35$ mV (where [AH] is the concentration of benzoic acid), becomes irreversible, and attains a stoichiometry of $2e^-$. Similar trends were obtained for $\mathbf{H_2CX^3}$**-Me**, as shown in *SI Appendix*, Fig. S3 *A* and *C*.

To gain insight into the product of the $2e^-$ reduction in the presence of acid, spectroelectrochemical studies were undertaken. Fig. 6 *A* and *B* shows the absorption profile obtained when solutions of $\mathbf{H_2CX^3}$**-Me** and $\mathbf{H_2CX^{10}}$**-Me**, respectively, were reduced in the presence of excess benzoic acid (50 mM) at a potential of −1.65 V vs. Fc^+/Fc. A very broad absorption band centered at λ_{max} = ~530 nm is observed. This ill-defined absorption profile is reminiscent of the only previous report of spectral data for a chlorinphlorin (10). As in porphyrins (5, 11, 18, 22), electrochemical reduction of the macrocycle results in dearomatization of the conjugated ring system, which should favor protonation of the *meso* carbon to afford a phlorin intermediate. To unequivocally confirm the formation of a chlorinphlorin, we sought to chemically reduce chlorin in the presence of acid and structurally characterize the resulting compound. A protonation–reduction sequence was achieved by reduction of *meso*-tetraphenylchlorin with cobaltocene subsequent to protonation using tosylic acid monohydrate. The crystal structure of the chlorinphlorin product is shown in Fig. 7. This represents an elusive example of a crystallographically characterized chlorinphlorin. The structure is distinguished by the tetrahedral geometry of the C(11) methine carbon. As shown in *SI Appendix*, Fig. S4,

Downloaded from https://www.pnas.org by Univ Joseph Fourier/INPG on September 5, 2024 from IP address 152.77.14.50.

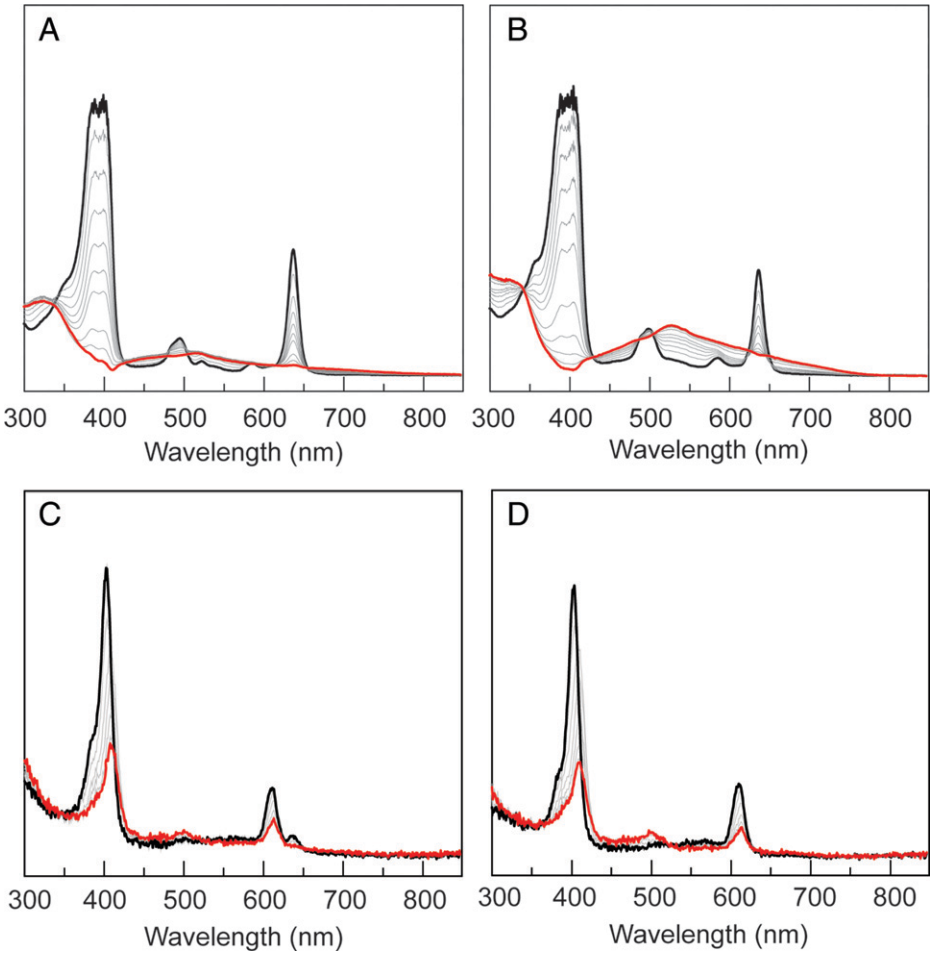

Fig. 6. Thin-layer UV-vis spectroelectrochemistry in acetonitrile with *n*-Bu_4NPF_6 (0.1 M) as the supporting electrolyte. Black traces show initial spectra, and red traces show the final spectra. (*A*) **H_2CX^3-Me** in the presence of excess benzoic acid (50 mM) at –1.65 V vs. Fc^+/Fc. (*B*) **H_2CX^{10}-Me** in the presence of excess benzoic acid (50 mM) at –1.65 V vs. Fc^+/Fc. (*C*) **$ZnCX^3$-Me** solution in the presence of excess benzoic acid (50 mM) at –1.70 V vs. Fc^+/Fc. (*D*) **$ZnCX^{10}$-Me** in the presence of excess benzoic acid (50 mM) at –1.70 V vs. Fc^+/Fc.

meso-tetraphenylchlorin exhibits the same reductive spectroelectrochemical behavior in the presence of acid (shown in Fig. 6) as for the hangman chlorins. Moreover, the ultraviolet-visible (UV-vis) absorption spectrum of the chemically prepared chlorinphlorin (*SI Appendix*, Fig. S4*B*) matches the observed spectroelectrochemical spectrum obtained from reduction of the compound (*SI Appendix*, Fig. S4*A*).

With the chlorinphlorin established as the PCET product of chlorin hydrogenation, the CVs of chlorin in the presence of exogenous acid are in accordance with the ECEC mechanism shown in Scheme 2, where each C step is a proton transfer from the benzoic acid in solution to the chlorin ring. For simplicity, **H_2CX^3-Me** and **H_2CX^{10}-Me** are represented by **Chl** in the mechanism. We propose that the first protonation occurs at nitrogen, characterized by the rate constant k_{H1}, and may be facilitated by hydrogen bonding with benzoic acid. From the position of the irreversible first wave in the presence of benzoic acid, the first protonation rate constant k_{H1} (Table 2) can be evaluated using (19)

$$E_p = E_1^0 - 0.78\frac{RT}{F} + \frac{RT}{2F}\ln\left(\frac{RT}{Fv}k_{H1}[\mathrm{AH}]\right). \qquad [2]$$

The neutral radical [**Chl(H)$^\bullet$**] obtained after the first EC sequence may be further reduced at the electrode, followed by a second proton transfer (k_{H2}) to furnish the *meso* C–H at the C(11) carbon of Fig. 7. Due to dearomatization caused by the first reduction, the second reduction is easier so that $E_{h1}^0 \gg E_1^0$. The small quasireversible wave observed at ∼–1.85 V vs. Fc^+/Fc results from the reduction of the hydrogenated chlorin, **Chl(H_2)**, formed after the second protonation. Consistent with this observation, a chemically synthesized tetraphenyl derivative shows a cathodic wave at –2.0 V vs. Fc^+/Fc; the shift of 150 mV may be the result of substituent effects. The low current associated with the **Chl(H_2)** reduction indicates that the second proton transfer is slow, as confirmed by two successive CV scans; the quasireversible wave attributed to the reduction of **Chl(H_2)** grows on the timescale of the second scan (*SI Appendix*, Fig. S5). The corresponding rate constant, $k_{H2} = 10$ M^{-1} s^{-1}, for this proton transfer (Table 2) is obtained from digital simulations of the CV of **H_2CX^{10}-Me** (Fig. 5*D*) and of **H_2CX^3-Me** (*SI Appendix*, Fig. S6) in the presence of benzoic acid. The anion **Chl(H)$^-$** is only partially stable on the timescale of the CV due to its slow protonation; its reoxidation (characterized by a standard potential E_{h1}^0) is assigned to the anodic wave at ∼–1.10 V vs. Fc^+/Fc.

The reduction of **$ZnCX^3$-Me** (*SI Appendix*, Fig. S7 *A* and *B*) and **$ZnCX^{10}$-Me** (*SI Appendix*, Fig. S7 *C* and *D*) in the presence of benzoic acid is also proton dependent in a fashion similar to **H_2CX^3-Me** (*SI Appendix*, Fig. S3 *A* and *C*) and **H_2CX^{10}-Me** (*SI Appendix*, Fig. S3 *B* and *D*). Using Eq. **2**, the k_{H1} listed in Table 2 are obtained. However, in contrast to the behavior of the free bases, reductive spectroelectrochemistry of

Downloaded from https://www.pnas.org by Univ Joseph Fourier/INPG on September 5, 2024 from IP address 152.77.14.50.

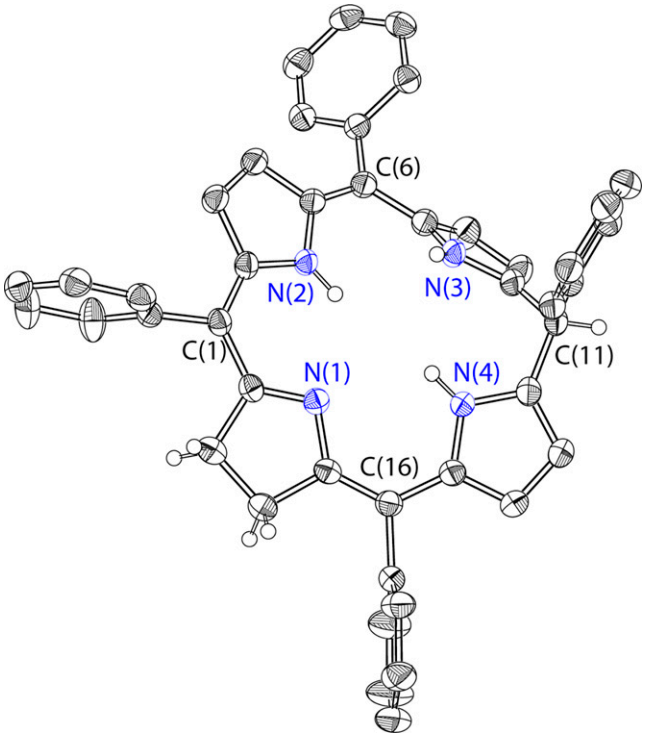

Fig. 7. Crystal structure of the synthesized chlorinphlorin. A hydrogen-bonded pyridine molecule and all nonoxidizable hydrogen atoms bound to carbon have been omitted for clarity.

ZnCX^3-Me (Fig. 6*C*) or **ZnCX^{10}-Me** (Fig. 6*D*) at –1.70 V vs. Fc^+/Fc in the presence of excess benzoic acid (50 mM) generates absorption spectra that are characteristic of isobacteriochlorins (23, 24). The coordination of zinc within the chlorin cavity precludes the formation of the initial N–H bond and subsequent formation of a chlorinphlorin.

The presence of a proximate proton perturbs the hydrogenation of the chlorin macrocycle. Fig. 8 shows the CVs of **H$_2$CX^{10}-H** in the presence of benzoic acid; the CVs of **H$_2$CX^3-H** in the presence of benzoic acid are shown in *SI Appendix*, Fig. S8. The effect of the proton in the hanging group is immediately obvious from the CV in the absence of benzoic acid (Figs. 4*B* and 8, red trace). The first reduction wave is irreversible, and moreover, the current of the second reduction wave is reduced. Per the specific site of protonation in the ECE mechanism of Scheme 1, the radical anion is neutralized by the transfer of a proton from the hanging group to the nitrogen of the macrocyclic ring to form the N–H bond. Comparing the rate constant of the first protonation (k_{H1} in Table 2) with the rate constant of the internal proton transfer from the hangman group (k_{PT} in Table 1) leads to the conclusion that the equivalent apparent acid concentration corresponding to the hangman group ($C_{app} = k_{PT}/k_{H1}$) is small at ~2 mM. With the addition of acid, even as low as <2 mM, an increase in the intensity of the first wave was observed along with a concomitant decrease in the subsequent reversible wave associated with the second reduction process.

At higher concentrations of acid (from 2 to 20 mM), the first wave shifts anodically and becomes a two-electron wave. The cathodic wave of **H$_2$CX^{10}-H** is ~125 mV more positive vs. that of **H$_2$CX^{10}-Me** in the presence of 20 mM benzoic acid. This shift rules out a stepwise electron-transfer/proton-transfer (ET/PT) process because application of Eq. **2** would imply a proton transfer rate constant k_{H1} at least four orders of magnitude larger than the value obtained with the **H$_2$CX^{10}-Me**. Carboxylic acid groups over a porphyrin macrocycle have been shown to preorganize molecules within the cleft via hydrogen bonding (25). Accordingly, as shown in Scheme 3, we propose that, due to hydrogen bonding, the pendant carboxylic acid group and imine *N*-atom facilitate the prepositioning of benzoic acid. The hydrogen bonding network supports a concerted PCET, thus circumventing the anion radical intermediate. We note that the rate constant (k_{CPET}) and the standard potentials (E^0_{CPET}) cannot be determined independently because the peak potential depends on both k_{CPET} and E^0_{CPET}:

$$E_p = E^0_{CPET} - 0.78\frac{RT}{\alpha F} + \frac{RT}{\alpha F}\ln\left(k_{CPET}[\mathrm{AH}]\sqrt{\frac{RT}{\alpha F v D}}\right), \quad [3]$$

where α is the transfer coefficient [$\alpha \sim 0.5$ evaluated from the wave width: $E_{p/2} - E_p = 1.857(RT/\alpha F)$ with $E_{p/2} - E_p \sim 100$ mV] (19). The shift of the wave upon the addition of benzoic acid is much more pronounced with the pendant acid functionality than for the chlorins with the ester group ($\partial E_p/\partial \log[\mathrm{AH}] \sim 150$ vs. 35 mV, respectively), consistent with a CPET mechanism for the former; PCET reduction for the pendant acid derivative is more facile, and this is also in line with the predicted shift for a concerted process $\frac{\partial E_p}{\partial \log[\mathrm{AH}]} = \frac{RT\ln 10}{\alpha F} \approx$ 120 mV/decade (Eq. **3**) as opposed to $\frac{\partial E_p}{\partial \log[\mathrm{AH}]} = \frac{RT\ln 10}{2F} \approx$ 30 mV/decade for a stepwise process (Eq. **2**). Note that, in the absence of acid, a stepwise ET/PT process (Scheme 1) prevails owing to a prohibitively long proton transfer distance. The structure of related Ni hangman porphyrin (26) shows a distance of 3.6 Å between the carboxylic acid proton and the nearest pyrrolic nitrogen, with the proton engaging in hydrogen bonding with the xanthene oxygen. This rather long distance between donor and acceptor, along with the high degree of deviation from linearity in the donor–proton–acceptor angle

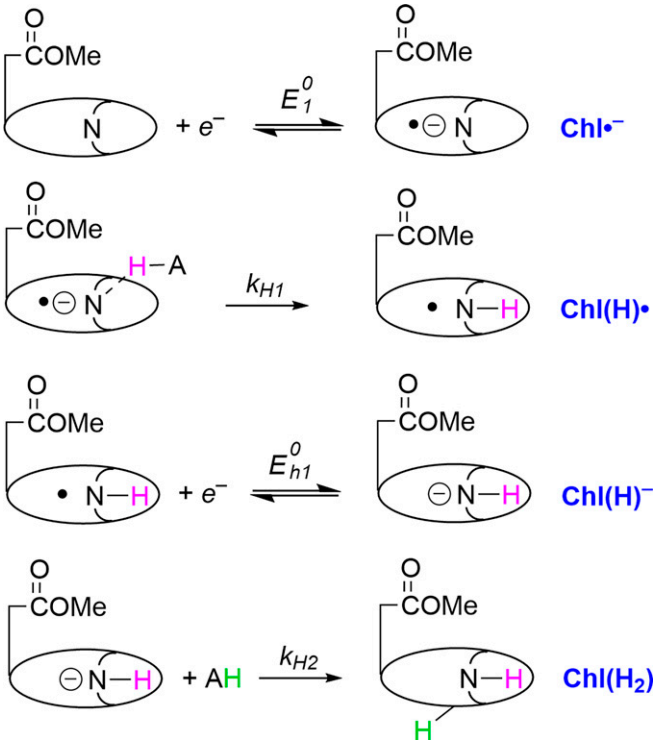

Scheme 2. Mechanism for the hydrogenation reduction of chlorin to furnish chlorinphlorin.

Downloaded from https://www.pnas.org by Univ Joseph Fourier/INPG on September 5, 2024 from IP address 152.77.14.50.

(106°) between the O–H–N groups, likely leads to a prohibitive kinetic barrier for concerted PCET. With the shortening of the proton tunneling distance upon binding acid within the cleft, the mechanism shifts from ET/PT to CPET.

Interestingly, the metallated chlorins, **ZnCX^3-H** and **ZnCX^{10}-H**, do not exhibit the same CV features as the corresponding free base chlorins **H$_2$CX^3-H** and **H$_2$CX^{10}-H**; at high concentrations of exogenous benzoic acid, no anodic shift of the first two-electron irreversible wave is observed when compared with **ZnCX^3-Me** and **ZnCX^{10}-Me**, and there is no substantial shift of the wave with increasing acid concentration (*SI Appendix*, Fig. S9), indicating that the **ZnCX^3-H** and **ZnCX^{10}-H** electrochemical hydrogenations follow a stepwise pathway akin to Scheme 2 to produce the isobacteriochlorin (Fig. 6 *C* and *D*) as opposed to the chlorinphlorin.

Conclusion

The electrochemical reduction of free base and zinc chlorins by PCET furnishes reduced macrocycles as a result of ligand noninnocence. Spectroelectrochemistry reveals that upon electrochemical hydrogenation, free base chlorins generate the rare chlorinphlorins, whereas zinc chlorins generate the more well-known isobacteriochlorins. The chlorinphlorin has unequivocally been established by its independent chemical preparation and X-ray structural characterization. Quantitative cyclic voltammetry analysis reveals that the apparent acid concentration corresponding to the hangman group is ∼2 mM, and the rate constant for proton transfer from the hanging group to the pyrrolic nitrogen of the free base chlorin is 10^3 s^{-1}. A synergetic effect between the exogenous acid and the hangman pendant carboxylic group facilitates PCET reduction as is evident when compared with the corresponding chlorin with an ester pendant group. We propose that a concerted PCET occurs when an exogenous proton donor is prepositioned by the pendant carboxylic acid to hydrogen bond to the *N*-atom within the chlorin core. Indeed, hangman complexes of porphyrin macrocycles have been shown to organize molecules between the pendant carboxylic acid group and the porphyrin macrocycle via hydrogen bonding networks that are reminiscent to those found in heme proteins (25–30). In this regard, the hangman group captures the hydrogen bonding environment of secondary coordination spheres of enzymatic tetrapyrrole cofactors, facilitating PCET via hydrogen bonding networks.

Table 2. Standard potentials (in V vs. Fc$^+$/Fc) and bimolecular proton transfer rate constants with benzoic acid (in molar^{-1} second^{-1})

Y = Me	H$_2$CX^{10}-Y	ZnCX^{10}-Y	H$_2$CX^3-Y	ZnCX^3-Y
E^0_1	−1.68	−1.88	−1.65	−1.86
E^0_2	−2.12	−2.22	−2.05	−2.16
E^0_{h1}	>−1.00	—	>−1.00	—
E^0_{h2}*	−1.85	−2.05	−1.85	−2.07
k_{H1}	5 × 10^5	5 × 10^4	5 × 10^5	2 × 10^4
k_{H2}	10	—	10	—

*Potential at which the chlorinphlorin, Chl(H$_2$), is reduced to Chl(H$_2$)$^{\bullet-}$. This reduction is not shown in Scheme 2.

Experimental

General Considerations. Acetonitrile was purified and dried through a neutral alumina column under argon. The supporting electrolyte, *n*-Bu$_4$NPF$_6$, was purchased from Sigma Aldrich (>99%), recrystallized from a water–ethanol mixture, and dried. All other chemicals were used as received. Chlorins and hangman chlorins were prepared according to previously reported procedures (7). CVs were collected using a CH Instruments potentiostat. Chlorins were dissolved in a solution containing *n*-Bu$_4$NPF$_6$ (0.1 M) as the supporting electrolyte. A three-electrode cell configuration was used with a platinum wire counterelectrode, a nonaqueous Ag$^+$/Ag reference electrode, and a glassy carbon working electrode that was meticulously polished before each measurement. The polishing procedure was performed on felt using different diamond pastes of different sizes (15, 6, 3, and 1 μm). The electrode was briefly sonicated in ethanol and dried under a stream of compressed air before use. The working electrodes were repolished with 1-μm diamond paste in between CV measurements. Ohmic drop was compensated for using the positive feedback compensation implemented in the instrument. All potentials are reported vs. the Fc$^+$/Fc redox couple. Thin-layer

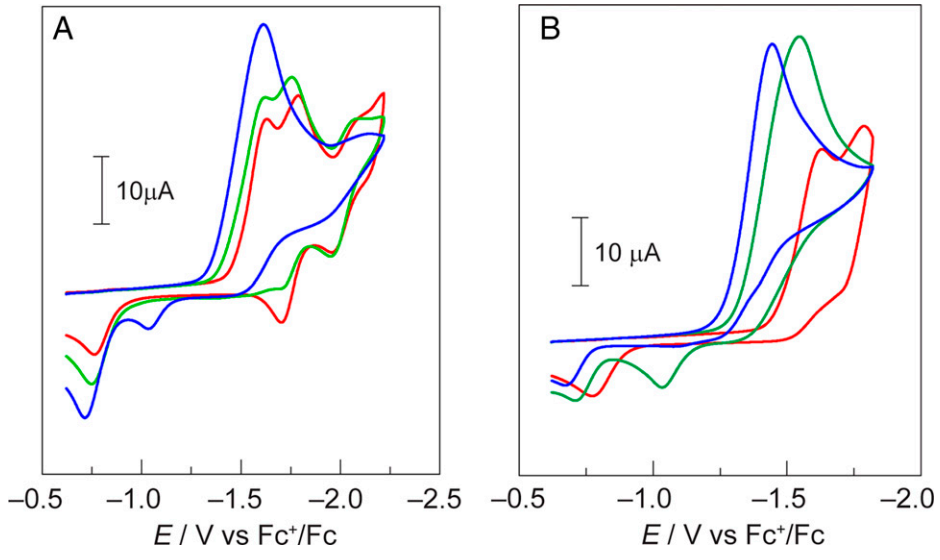

Fig. 8. CVs of **H$_2$CX^{10}-H** (2.0 mM) in the presence of benzoic acid at concentrations of (*A*) 0 mM (red), 0.5 mM (green), and 2 mM (blue) and (*B*) 0 mM (red), 5 mM (green), and 20 mM (blue). All CVs were taken in anhydrous acetonitrile with *n*-Bu$_4$NPF$_6$ as the supporting electrolyte (0.1 M) using a 3-mm glassy carbon working electrode. v = 0.1 V/s.

Downloaded from https://www.pnas.org by Univ Joseph Fourier/INPG on September 5, 2024 from IP address 152.77.14.50.

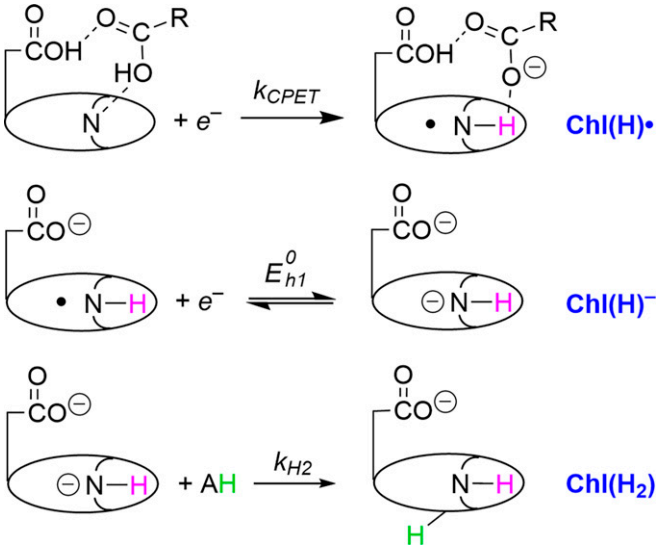

Scheme 3. Mechanism for the PCET hydrogenation of hangman chlorin to furnish chlorinphlorin.

spectroelectrochemistry data were recorded in an N_2-filled glove box on an Ocean Optics spectrometer with a 0.5-mm path-length quartz cell, a Pt mesh working electrode, a Pt wire counterelectrode, and a nonaqueous Ag^+/Ag reference electrode, all of which were purchased from BioAnalytical Systems. UV-vis-NIR (near-infrared) spectra were recorded at room temperature in quartz cuvettes on a Varian Cary 5000 UV-vis-NIR spectrophotometer. Simulations were performed using the DigiElch program (31) using the mechanism in *SI Appendix*, Scheme S1; results are summarized in *SI Appendix*, Table S1.

Synthesis of *Meso*-Tetraphenylchlorinphlorin. In an N_2-filled glove box, *meso*-tetraphenylchlorin (30.0 mg, 0.0486 mmol) was dissolved in 5 mL of dichloromethane (DCM), and tosylic acid monohydrate (9.2 mg, 0.049 mmol) was added as a solid. The reaction mixture was stirred for 2 h at room temperature, and cobaltocene (9.2 mg, 0.049 mmol) was subsequently added dropwise as a solution in DCM (~2 mL). The resulting violet solution was stirred for 15 min. This procedure was repeated with a second equivalent of tosylic acid monohydrate (9.2 mg, 0.049 mmol) and cobaltocene (9.2 mg, 0.049 mmol). The solvent was then concentrated in vacuo, and the product was purified under an N_2 atmosphere by preparatory thin-layer chromatography on silica with DCM as the mobile phase. The titular compound was isolated as a violet powder (23 mg, 77%). Crystals for X-ray crystallography were grown by vapor diffusion of hexanes into a pyridine solution of the compound. ^{1}H and ^{13}C NMR spectra are shown in *SI Appendix*, Fig. S10: ^{1}H NMR (400 MHz, CD_2Cl_2): δ 7.63 (dd, J = 7.8, 1.7 Hz, 2H), 7.50 to 7.33 (m, 13H), 7.30 (br, 1H), 7.20 to 7.09 (m, 3H), 7.00 (d, J = 5.2 Hz, 2H), 6.90 (d, J = 7.9 Hz, 2H), 6.62 (t, J = 2.6 Hz, 1H), 6.60 to 6.54 (m, 3H), 6.51 (t, J = 3.1 Hz, 1H), 6.29 (s, 1H), 6.01 (t, J = 2.8 Hz, 1H) 2.84 to 2.55 (m, 4H); ^{13}C NMR (101 MHz, CD_2Cl_2): δ 152.1, 151.4, 142.6, 141.4, 140.6, 140.3, 135.8, 134.1, 133.0, 132.5, 131.3, 131.2, 129.2, 128.81, 128.78, 128.6, 128.3, 127.61, 127.60, 127.3, 126.5, 125.4, 124.3, 120.9, 119.7, 116.5, 115.4, 112.0, 111.0, 109.3, 106.4, 44.6, 36.4, 30.4; high-resolution mass spectrometry (electrospray ionization) mass-to-charge ratio: calculated for $[M + H]^+$ ($M = C_{44}H_{34}N_4$) 619.2856, found 619.2843.

X-Ray Crystallography Details. X-ray diffraction data were collected at the Advanced Photon Source at the Argonne National Laboratory on a Huber three-circle goniometer with free-κ using a Pilatus 1M CdTe Pixel Array Detector and an Oxford Cryosystems cryostat operating at 100 K. A synchrotron X-ray source with a wavelength of 0.41328 Å was used. The crystal was mounted on a cryoloop using Paratone oil. Data were integrated using SAINT, and multiscan absorption correction was applied using SADABS. The structure was solved by intrinsic phasing using SHELXT (APEX3 program suite 2016) and refined against F^2 on all data by full matrix least squares with SHELXL. All atoms were located in the difference-Fourier maps, and all nonhydrogen atoms were refined anisotropically. The crystal structure with the difference-Fourier map (green) used to locate hydrogen atoms bound to pyrrolic nitrogen atoms is shown in *SI Appendix*, Fig. S11. Crystal data and structure refinement for *meso*-tetraphenylchlorinphlorin are listed in *SI Appendix*, Table S2.

Data Availability. Crystal structure data have been deposited in the Cambridge Crystallographic Data Centre (CCDC, accession no. 2126181). All other data are included in the manuscript and/or *SI Appendix*.

ACKNOWLEDGMENTS. This material is based upon work supported under Solar Photochemistry Program of the Chemical Sciences, Geosciences and Biosciences Division, Office of Basic Energy Sciences of the US Department of Energy (DOE) Grant DE-SC0017619. Use of the Advanced Photon Source, an Office of Science User Facility operated for the DOE Office of Science by the Argonne National Laboratory, was supported by DOE Contract DE-AC02-06CH11357.

Author affiliations: [a]Department of Chemistry and Chemical Biology, Harvard University, Cambridge, MA 02138; [b]Université Grenoble Alpes, CNRS, Grenoble, 38000 France; and [c]Université Paris Cité, Paris, 75013 France

1. H. Tamiaki, M. Teramura, Y. Tsukatani, Reduction processes in biosynthesis of chlorophyll molecules: Chemical implication of enzymatically regio- and stereoselective hydrogenations in the late stages of their biosynthetic pathway. *Bull. Chem. Soc. Jpn.* **89**, 161–173 (2015).
2. N. Muraki *et al.*, X-ray crystal structure of the light-independent protochlorophyllide reductase. *Nature* **465**, 110–114 (2010).
3. J. Derosa, P. Garrido-Barros, J. C. Peters, Electrocatalytic reduction of C–C π bonds via a cobaltocene-derived concerted proton-electron transfer mediator: Fumarate hydrogenation as a model study. *J. Am. Chem. Soc.* **143**, 9303–9307 (2021).
4. C. Costentin, J. M. Savéant, C. Tard, Ligand "noninnocence" in coordination complexes vs. kinetic, mechanistic, and selectivity issues in electrochemical catalysis. *Proc. Natl. Acad. Sci. U.S.A.* **115**, 9104–9109 (2018).
5. B. H. Solis, A. G. Maher, D. K. Dogutan, D. G. Nocera, S. Hammes-Schiffer, Nickel phlorin intermediate formed by proton-coupled electron transfer in hydrogen evolution mechanism. *Proc. Natl. Acad. Sci. U.S.A.* **113**, 485–492 (2016).
6. A. G. Maher, M. Liu, D. G. Nocera, Ligand non-innocence in nickel porphyrins: Nickel isobacteriochlorin formation under hydrogen evolution conditions. *Inorg. Chem.* **58**, 7958–7968 (2019).
7. H. H. Inhoffen, P. Jäger, R. Mählhop, C. D. Mengler, Zur weiteren kenntnis des chlorophylls und des hämins, XII. Elektrochemische reduktionen an porphyrinen und chlorinen, IV. *Justus Liebigs Ann. Chem.* **704**, 188–207 (1967).
8. H. H. Inhoffen, P. Jäger, R. Mählhop, Further knowledge of chlorophyll and of hemin. 32. Partial synthesis of rhodin-G7-trimethyl ester from chlorin-E6-trimethyl ester and at same time completion of Harvard synthesis of chlorophyll a to chlorophyll b. *Justus Liebigs Ann. Chem.* **749**, 109 (1971).
9. V. P. Suboch *et al.*, Structure of products of chlorin photoreduction reaction. *Dokl. Akad. Nauk SSSR* **204**, 404 (1972).
10. A. A. Krasnovskii, Obratimoe fotokhimicheskoe vosstanovlenie khlorofilla askorbinovoi kislotoi. *Dokl. Akad. Nauk SSSR* **60**, 421–424 (1948).
11. H. H. Scheer, "Inhoffen, hydroporphyrins: Reactivity, spectroscopy, and hydroporphyrin analogues" in *The Porphyrins*, D. Dolphin, Ed. (Academic Press, New York, NY, 1978), pp. 45–90.
12. M. Taniguchi, M. Ptaszek, B. E. McDowell, P. D. Boyle, J. S. Lindsey, Sparsely substituted chlorins as core constructs in chlorophyll analogue chemistry. Part 3: Spectral and structural properties. *Tetrahedron* **63**, 3850–3863 (2007).
13. M. Taniguchi, J. S. Lindsey, Synthetic chlorins, possible surrogates for chlorophylls, prepared by derivatization of porphyrins. *Chem. Rev.* **117**, 344–535 (2017).
14. C. Costentin, Electrochemical approach to the mechanistic study of proton-coupled electron transfer. *Chem. Rev.* **108**, 2145–2179 (2008).
15. J. Heinze, "Aliphatic and aromatic hydrocarbons" in *Organic Electrochemistry, Revised and Expanded*, O. Hammerich, B. Speiser, Eds. (CRC Press, Boca Raton, FL, ed. 5, 2016), pp. 861–889.

Downloaded from https://www.pnas.org by Univ Joseph Fourier/INPG on September 5, 2024 from IP address 152.77.14.50.

16. C. Costentin, M. Robert, J. M. Savéant, Concerted proton-electron transfers: Electrochemical and related approaches. *Acc. Chem. Res.* **43**, 1019–1029 (2010).
17. M. Liu, D. K. Dogutan, D. G. Nocera, Synthesis of hangman chlorins. *J. Org. Chem.* **85**, 5065–5072 (2020).
18. G. S. Wilson, G. Peychal-Heiling, Electrochemical studies of tetraphenylporphin, tetraphenylchlorin, and tetraphenylbacteriochlorin. *Anal. Chem.* **43**, 550–556 (1971).
19. J. M. Savéant, C. Costentin, *Elements of Molecular and Biomolecular Electrochemistry* (John Wiley & Sons, Hoboken, NJ, ed. 2, 2019).
20. C. Amatore, J. M. Savéant, Electrochemical hydrogenation of aromatic hydrocarbons: Discrimination between ECE and disproportionation mechanisms by double potential step chronoamperometry. *J. Electroanal. Chem. Interfacial Electrochem.* **107**, 353–364 (1980).
21. K. Izutsu, *Electrochemistry in Nonaqueous Solutions* (John Wiley & Sons, Hoboken, NJ, 2009).
22. B. H. Solis *et al.*, Theoretical analysis of cobalt hangman porphyrins: Ligand dearomatization and mechanistic implications for hydrogen evolution. *ACS Catal.* **4**, 4516–4526 (2014).
23. S. Singh *et al.*, Synthesis and photophysical properties of thioglycosylated chlorins, isobacteriochlorins, and bacteriochlorins for bioimaging and diagnostics. *Bioconjug. Chem.* **21**, 2136–2146 (2010).
24. Y. Yu, *et al.*, Stable iso-bacteriochlorin mimics from porpholactone: Effect of a β-oxazolone moiety on the frontier π-molecular orbitals. *Inorg. Chem. Front.* **2**, 671–677 (2015).
25. C. Y. Yeh, C. J. Chang, D. G. Nocera, "Hangman" porphyrins for the assembly of a model heme water channel. *J. Am. Chem. Soc.* **123**, 1513–1514 (2001).
26. D. K. Bediako *et al.*, Role of pendant proton relays and proton-coupled electron transfer on the hydrogen evolution reaction by nickel hangman porphyrins. *Proc. Natl. Acad. Sci. U.S.A.* **111**, 15001–15006 (2014).
27. J. D. Soper, S. V. Kryatov, E. V. Rybak-Akimova, D. G. Nocera, Proton-directed redox control of O-O bond activation by heme hydroperoxidase models. *J. Am. Chem. Soc.* **129**, 5069–5075 (2007).
28. J. Rosenthal, D. G. Nocera, Role of proton-coupled electron transfer in O-O bond activation. *Acc. Chem. Res.* **40**, 543–553 (2007).
29. J. Rosenthal, D. G. Nocera, Oxygen activation chemistry of pacman and hangman porphyrin architectures based on xanthene and dibenzofuran spacers. *Prog. Inorg. Chem.* **55**, 483–544 (2007).
30. C. M. Lemon, D. K. Dogutan, D. G. Nocera, "Porphyrin and corrole platforms for water oxidation, oxygen reduction and peroxide dismutation" in *Handbook of Porphyrin Chemistry*, K. M. Kadish, K. M. Smith, R. Guilard, Eds. (Academic Press, Amsterdam, the Netherlands, 2012), vol. 21, chap. 99, pp. 1–143.
31. M. Rudolph, Digital simulations on unequally spaced grids. Part 2. Using the box method by discretisation on a transformed equally spaced grid. *J. Electroanal. Chem. (Lausanne)* **543**, 23–39 (2003).

Downloaded from https://www.pnas.org by Univ Joseph Fourier/INPG on September 5, 2024 from IP address 152.77.14.50.